Journal of the European Ceramic Society **14** (1994) 245–255

Chemical Vapour Infiltration of TiB_2 and TiN in Porous Al_2O_3

J. P. Dekker,[a,b,*] P. J. van der Put,[a] H. J. Veringa[b] & J. Schoonman[a]

[a] Laboratory for Applied Inorganic Chemistry, Delft University of Technology, Juilianalaan 136, 2628 BL Delft, The Netherlands
[b] ECN, Energy Research Foundation, Westerduinweg 3, 1755 ZG Petten, The Netherlands

(Received 1 November 1993; accepted 31 January 1994)

Abstract

The mechanical strength of a porous material can be improved by deposition of a thin layer at the internal surface of the preform by chemical vapour infiltration (CVI). The influence of a CVI modification on the permeability and mechanical strength of porous alumina supports for porous alumina membranes for liquid filtration have been investigated. Numerical solutions of a mathematical description of a CVI process in an open cylinder are used to evaluate the influence of some process parameters on the infiltration kinetics. These results are used to explain the observed changes in permeability and mechanical properties. Porous alumina substrates can effectively be modified with titanium nitride (TiN) or titanium diboride (TiB_2) by CVI. The amount of deposited material in the substrate is determined by a combination of process parameters. Mathematical CVI model predictions indicate that a low growth rate constant and a high diffusion are beneficial for the infiltration of the deposit into the substrate, and that the surface growth rate kinetics of the deposit has an influence on the infiltration kinetics.

Die mechanische Festigkeit eines porösen Materials kann durch das Aufbringen einer dünnen Schicht auf die internen Grenzflächen, mittels chemischer Dampfinfiltration (CVI), verbessert werden. Der Einfluß der CVI Modifikation auf die Permeabilität und die mechanische Festigkeit von porösen Aluminiumoxidmembranen zur Filterung von Flüssigkeiten wurde untersucht. Unter Benutzung der numerischen Ergebnisse einer mathematischen Beschreibung des CVI Prozeßes für einen offenen Zylinder, wird der Einfluß verschiedener Prozeßparameter auf die Infiltrationskinetik untersucht. Die Ergebnisse werden zur Erklärung der beobachteten Veränderungen in der Permeabilität und den mechanischen Eigenschaften benutzt. Poröses Aluminiumoxidsubstrat kann mit Hilfe von CVI durch Titannitrid (TiN) oder Titandiborid (TiB_2) entscheidend verändert werden. Die Menge an eingelagertem Material im Substrat hängt von der Kombination der Prozeßparameter ab. Mathematische CVI Modellrechnungen zeigen, daß eine niedrige Wachstumsrate und starke Diffusion von Vorteil für die Infiltration sind und daß die Oberflächenwachstumskinetik der Einlagerung einen Einfluß auf die Infiltrationskinetik hat.

On peut améliorer la tenue mécanique de matériaux poreux en déposant sur la surface de la porosité une fine couche par infiltration chimique en phase vapeur (ICPV). L'influence d'une modification par ICPV sur la perméabilité et la résistance mécanique de supports poreux d'alumine pour des membranes poreuses d'alumine destinées au filtrage de liquides a été étudiée. On utilise les solutions numériques d'un modèle de déposition par ICPV dans un cylindre ouvert pour évaluer l'influence de certains paramètres de fabrication sur la cinétique de l'infiltration. On utilise ces résultats pour expliquer les variations de la perméabilité et des propriétés mecaniques. On peut par exemple modifier efficacement des substrats poreux d'alumine avec du nitrure de titane (TiN) ou du diborure de titane (TiB_2) infiltré par ICPV. La quantité de matériau déposé dans le substrat dépend de plusieurs paramètres de fabrication. D'après le modèle, une diffusion élevée et une constante de croissance faible favorisent l'infiltration, et le taux de déposition a une influence sur la cinétique d'infiltration.

Notation

A	Cross-sectional surface area of the C-ring (m^2)
C_1	Knudsen permeability fit constant (mol/(m^2 s Pa))

* Present address: Philips Centre for Manufacturing Technology, P.O. Box 218, 5600 MD Eindhoven, The Netherlands.

Journal of the European Ceramic Society 0955-2219/94/$7.00

C_2 Viscous flow permeability fit constant (mol/(m^2 s Pa^2))
C_3 Fit constant related to the strength of the untreated C-ring (MPa)
C_4 Strengthening fit constant (MPa)
C_i Concentration of species i (mol/m^3)
F Applied load in C-ring compression test (N)
J Mass flux (mol/s)
L Length of the substrate (m)
m Weibull modulus
m_t Measured mass increase of the substrate (g)
M Moment of inertia of a compressed C-ring (m)
M_s Molecular weight of the deposit (g/mol)
n Rank number of particular specimen for the Weibull analysis
N Total number of substrates used for the mechanical testing
p Gas permeability (mol/(m^2 s Pa))
P Probability of failure
P_1 Pressure of the feed (Pa)
P_2 Pressure of the permeate (Pa)
r Radius (m)
r_a Average radius of the C-ring (m)
r_i Inner radius of the C-ring (m)
r_o Outer radius of the C-ring (m)
R Surface growth rate of the deposit (mol/(m^2 s))
S Geometrical surface area of the substrate (m^2)
STP Standard temperature (273·15 K) and pressure (1×10^5 Pa)
V Volume of the substrate (m^3)
x Dummy variable for integration
X Densification factor

ε Porosity of the untreated substrates
θ Angle between the radius r and the normal of the load in the C-ring test.
ρ Density of the deposit (g/m^3)
σ_o Scaling parameter (MPa unit volume)
σ_X Calculated strength at a densification X (MPa)
σ_θ Stress at angle θ and radius r for a compressed C-ring (Pa)
σ_θ^{max} Maximum stress at failure for a compressed C-ring (Pa)

Introduction

Porous ceramic materials can be used for various applications, because of their chemical resistance and high-temperature stability. For example, they can act as an inorganic membrane for liquid and gas separation.[1,2] These membranes have to be as thin as possible to minimize the fluid resistance. These thin layers must be mechanically supported in order to withstand the applied transmembrane pressure difference. Thus, the resulting asymmetric system should consist of a thin membrane layer superimposed on a support with a high fluid permeability and good mechanical properties. A low fluid resistance of the support can be obtained by applying a coarse pore structure with a high porosity. However, such porosity is detrimental to the strength of a porous ceramic material.[3–6] An optimum between the two properties should be chosen depending on the final application. The mechanical strength of a porous material can be improved by deposition of a thin layer at the internal surface of the preform by the chemical vapour infiltration (CVI) process. In contrast to sintered ceramic materials these deposits originating from gaseous reactants are microcrystalline, and may have a fully dense structure.[7,8] In CVI gaseous species react to form a solid product at the internal surface of the porous preform. As a consequence, the preform densifies until there is no open porosity any more. Such a composite exhibits excellent mechanical properties with a high strength and toughness.[9] However, in the present paper, the density of the preform is purposely maintained at less than full density, resulting in a structure with enhanced mechanical properties and yet a considerable permeability. The influence of CVI modification on the properties of porous alumina (Al_2O_3) supports for porous Al_2O_3 membranes have been investigated.

Porous Al_2O_3 membranes for liquid filtration have been developed at the Netherlands Energy Research Foundation.[10] The membrane consists of a tubular porous support with a thin microfiltration layer on the inside. The tubular substrates are formed by extrusion of a ceramic paste which consists of a coarse α-Al_2O_3 powder, an inorganic binder (fine γ-Al_2O_2 powder), an organic binder, a lubricant, and water. These extruded tubes are dried and sintered in air.[10,11] The sintered porous alumina tubular substrates are infiltrated with TiN or TiB_2 by means of CVI. Some physical properties of the individual composite materials are listed in Table 1.

The good electrical conductivity of the infiltrated material can be used to our advantage to improve the separation performance of the membrane. The fluid flux through pressure driven ceramic membranes should be kept as high as

Table 1. Some physical properties of Al_2O_3, TiN and TiB_2

	Young's modulus (GPa)	*Thermal expansion (10^{-6} K^{-1})*[a]	*Density (10^3 kg/m^3)*	*Electrical resistivity (Ωm)*
Al_2O_3	366	9·1	3·90	$>10^4$
TiN	590	10	5·22	$4–15 \times 10^{-3}$
TiB_2	551	8·4	4·52	$9–15 \times 10^{-4}$

[a] At 1000 K.

possible. However, the build-up of retained species at the membrane surface can have a deleterious effect on the membrane flux. This concentration polarization of retained species can be avoided by electrophoretic techniques.[12] In an electrofiltration process the applied electric field across the membrane introduces an electrophoretic force opposite to that of the transmembrane pressure difference. The electric field will remove or disrupt the concentration polarization layer at the membrane surface. The combination of the filtration properties of the membrane with the electric field will determine the performance of such a system.[12] Conventionally, two noble metal electrodes are positioned on each side of the membrane.[12,13] In principle, the TiN or TiB_2 layer at the internal surface of the preform might act as an electrode, herewith reducing the electrode distance and simplifying the geometry of the final set-up. Thus, the modified support can act as an electrode for electrofiltration, and has enhanced mechanical properties.

A mathematical description of a CVI process in an open cylinder under isothermal and isobaric conditions is used to evaluate the influence of some process parameters on the infiltration kinetics. Numerical modelling of a CVI process has been proven to give a better understanding of the influence of the process parameters on the densification.[14–16] The theoretical model for the evaluation of the CVI process describes the mass balance of the diffusing gaseous reactants in combination with the surface growth rate in the cylinder, and the numerical solution procedure takes into account the changing pore geometry due to the formation of a solid at the inside of the cylinder. Detailed discussions of the model are given elsewhere.[15,16] The influence of growth rate constant, reactant concentration, and process time on the densification are evaluated.

The distribution of the deposits in the pore network is studied with scanning electron microscopy (SEM) and energy dispersive X-ray (EDX) analysis. These experimental results along with some numerical CVI model calculations are discussed, and the change in gas permeability and fracture strength of the support are discussed as a function of the synthesis conditions.

Table 2. Typical parameters used for the modelling of the CVI process for TiB_2 in a cylinder

Model parameters		*Cylinder*	
Pressure	10^5 Pa	Length	6 mm
Temperature	1 000 K	Radius	2·5 μm
Process time	3 000 s		
$TiCl_4$ concentration	0·446 mol/m^3 (STP)		
Growth rate constant	$1{\cdot}48 \times 10^{-4}$ m/s		

Experimental aspects

Mathematical model

Numerical solutions of the mathematical CVI model are used to evaluate the influence of growth rate constant, reactant concentration, and process time on the densification. The physical properties of $TiCl_4$, H_2, and TiB_2 are used for the model calculations. It is assumed that the growth rate is only first order in the $TiCl_4$ concentration, and that the depletion of H_2 and BBr_3 in the cylinder can be neglected. Typical parameters used for the model predictions for the deposition of TiB_2 in a cylinder are given in Table 2.

CVI experimental aspects

Two similar hot-wall CVD reactors are used for the synthesis experiments. There are only minor differences in the design of the reactor. The experimental results in the two reactors are comparable.[17] The CVD apparatus consists of a quartz tube with a diameter of 49 mm. The quartz tube of the other CVD apparatus is slightly smaller. The substrates are slid over a quartz rod which is positioned in the centre of the tubular reactor in order to ensure uniform distribution of the gas phase reactants around the substrate. A flat dense Al_2O_3 substrate is placed in the vicinity of the tubular substrate to monitor the surface growth rate. More detailed descriptions of the experimental conditions for the synthesis of TiN and TiB_2 in a hot-wall reactor have been given earlier.[17,18] The experimental conditions are summarized in Table 3.

The volume deposited in the porous substrate relative to the initial pore volume is used as a characteristic property of the modified substrates. This measure for the densification (X) can be determined using

$$X = \frac{m_t - (1 - \varepsilon)SM_sRt}{\varepsilon\rho V} \qquad (1)$$

where m_t is the measured mass increase, ε the initial porosity, S the external geometrical surface area, M_s the molecular weight of the deposit, R the surface growth rate, t the process time, ρ the density of the deposit, and V the volume of the porous preform. It should be noted that X cannot discriminate between the differences in the homogeneity of the deposit within the pore network of the substrate.

EDX analysis

An EDX analyser (EDAX PV 9100) in combination with an SEM (JEOL JSM-35) is used to determine the distribution of the deposit within the porous substrate. Small surface areas at a fracture plane are characterized using the relevant condi-

Table 3. Experimental standard conditions for the synthesis of TiN and TiB_2 in tubular porous Al_2O_3 substrates

Parameters		*TiN*	*TiB_2*		*Substrate*	
C_{TiCl_4}	(STP)[a]	0·2–0·8	0·134	mol/m^3	Length	15 mm
C_{BBr_3}	(STP)	—	0·267	mol/m^3	Outer diameter	15 mm
C_{N_2}	(STP)	11–22	—	mol/m^3		
C_{H_2}	(STP)	11–22	22·1	mol/m^3	Inner diameter	9 mm
C_{Ar}	(STP)	—	22·1	mol/m^3		
Flow	(STP)	0·4–0·8	0·6–0·8	mol/m^2 s	*r*(average)[b]	2·3 μm
Pressure		1	0·1–1	10^5 Pa	Porosity[b]	0·385
Temperature		1073–1273	823–1073	K		
Process time		1·8–21·6	3·6–28·8	10^3 s		

[a] Input reactant concentration.
[b] Derived from Hg-porosimetry.

tions for the instrumentation as given in CEN/TC184.[19] Surface scans (0·08 mm^2) are employed to average out differences in the local take-off angle of the characteristic X-ray which is unknown due to the surface roughness of the fractured cross-section. The cumulative intensity after 60 s life-time at a region of 240 eV around the TiKα energy (4·51 keV) is used as a measure for the amount of material deposited within the substrate at a given position. These measurements are performed as a function of the radius at half axial length at a fractured cross-section of the tubular substrate as illustrated in Fig 1. The recorded TiKα intensities are divided by the measured AlKα intensity of a standard in order to correct for any fluctuations in the instrument conditions.

Permeability

The increase in fluid resistance after infiltration is measured using forced flow inert gas (argon or helium) permeability measurements at room temperature. The permeability (p) can be defined as

$$p = \frac{J}{S(P_1 - P_2)} \tag{2}$$

where J is the mass flux, P_1 is the high pressure of the feed, and P_2 is the low pressure of the permeate. The permeability is proportional to the average pressure

$$p = C_1 + C_2 \frac{(P_1 + P_2)}{2} \tag{3}$$

where C_1 and C_2 are constants which are attributed to the Knudsen flow and viscous flow, respectively. The argon permeability is measured as a function of the average pressure before and after each modification. The relative permeability, i.e. the ratio of the permeability after modification over the original permeability, at an average pressure of 7×10^4 Pa is used as a measure for the infiltration characteristics. The change in this relative permeability is studied as a function of the synthesis conditions.

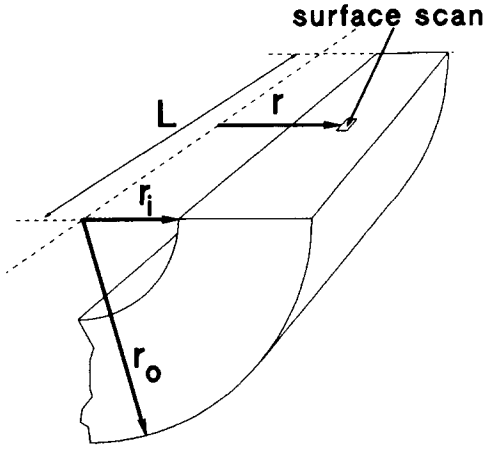

Fig 1. Schematic presentation of the geometry used for the EDX analysis where surface scans are applied as a function of *r*.

Mechanical testing

A C-ring diametral compression test[20,21] is used to study the influence of the amount of deposited material on the strength of the tubular substrate. A C-ring compression test is chosen, because the stress distribution in this testing configuration is close to the actual stress distribution under process conditions.[22] The specimens are fractured at a crosshead speed of 4–5 μm/s at room temperature. The tangential stress $\sigma(r, \theta)$ for isotropic material in a compressed C-ring can be calculated using the following equations:[20,21]

$$\sigma(r, \theta) = \frac{M(r - r_a)F}{r(M - r_a)A} \cos(\theta) \tag{4}$$

$$r_a = \frac{(r_o + r_i)}{2} \tag{5}$$

$$M = \frac{(r_o - r_i)}{\ln\left(\frac{r_o}{r_i}\right)} \tag{6}$$

$$A = (r_o - r_i)L \tag{7}$$

where M is the moment of inertia, F the load, r_i the inner diameter, r_o the outer diameter, L the length, A the cross-sectional surface area, and θ

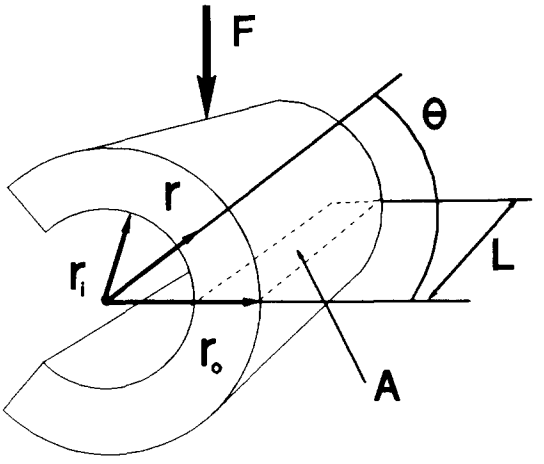

Fig. 2. Schematic presentation of a C-ring diametral compression test.

the angle between r and the normal of the load as illustrated in Fig 2. The maximum stress at failure can be calculated by monitoring the load, and measuring the angle between the fracture plane and the normal of the load. These stress calculations hold for uniform material. However, the modified substrates are inherently anisotropic. Thus, the calculated maximum stress at failure is not the real maximum stress. As a consequence, the mechanical testing results can only be used qualitatively. The relative strength defined as the ratio of the calculated maximum stress for the modified substrate over the average maximum stress of the untreated substrates is studied as a function of the synthesis conditions. Weibull statistics are used to discuss the influence of the modification on the fracture probability.

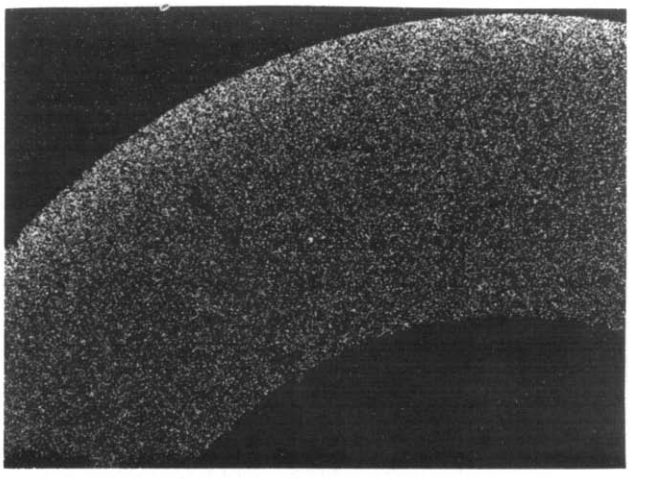

(a)

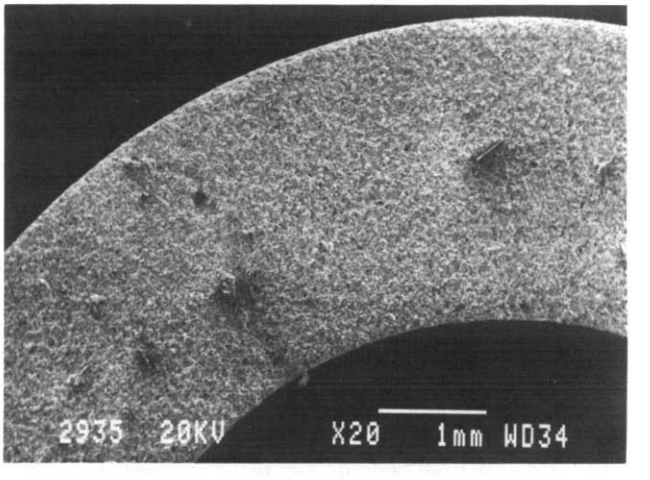

(b)

Fig. 3. (a) TiKα EPMA mapping, and (b) SEM micrograph of a substrate modified with TiN at a reaction temperature of 1123 K.

Results and discussion

Synthesis results

A characteristic result of the CVI experiments is presented in Figs 3(a) and 3(b). The presented TiKα EPMA mapping of a cross-section of a TiN modified substrate clearly indicates the expected decrease in the amount of deposited material into the substrate. An SEM micrograph of a cross-section of a TiN modified substrate, the corresponding TiKα EPMA mapping, and a SEM micrograph of an untreated substrate for comparison are presented in Figs 4(a)–(c), respectively. From these figures it can be concluded that the microstructural characteristics of the pore network remain unchanged after modification. The deposit is smoothly distributed over the coarse and fine Al_2O_3 particles.

The origin of the mass increase of the inert substrate during the CVI process can be ascribed to two different mechanisms, i.e. the surface reaction at the outer surface and the surface reaction at the internal surface of the substrate. At the outer surface the mass increase rate is independent of time, whereas at the inner surface the mass increase rate decreases with time. The mass increase in the pore network is determined by a combination of mass transfer in the gas phase and growth rate at the internal surface, and with increasing densification the pore size will decrease which will reduce the mass flux into the pore. The contribution of the mass increase at the outer surface was always less than 20% with respect to the total measured mass increase. Thus, the measured mass increase is mainly determined by the growth rate at the internal surface.

The measured mass increases for TiN and TiB_2 as a function of time are given in Fig. 5. It is coincidental that the observed mass increases for the synthesis of TiN and TiB_2 are comparable, because the surface growth rates, reaction temperature, and reactant concentrations are very different. The surface growth rate for TiN is $0{\cdot}85 \times 10^{-4}$ mol/(m^2s) at 1073 K using a $TiCl_4$ input concentration of 0·446 mol/m^3, whereas the surface

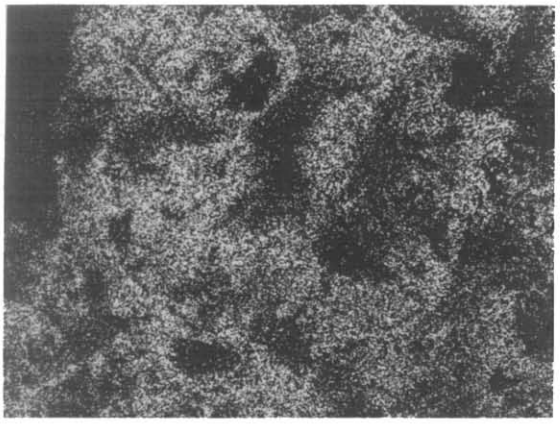

(a)

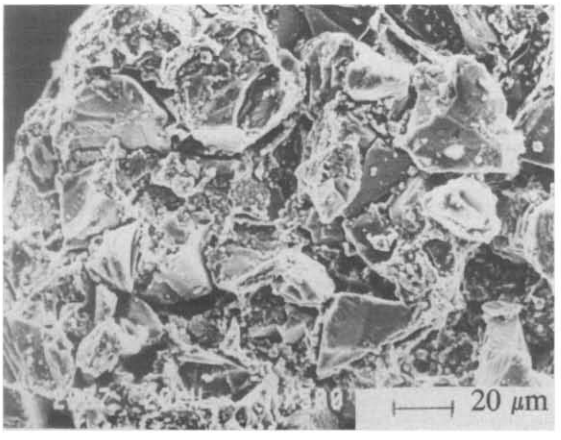

(b)

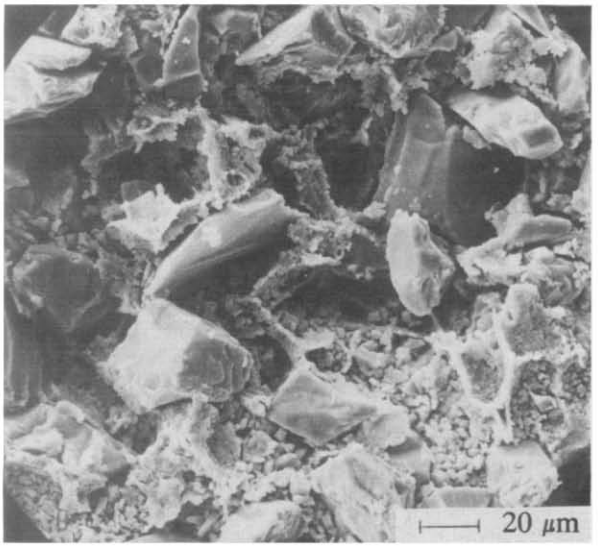

(c)

Fig. 4. (a) A TiKα EPMA mapping, and (b) SEM micrograph of a cross-section near the outside of a TiN modified substrate, and (c) SEM micrograph of an untreated substrate for comparison.

growth rate for TiB_2 is $1{\cdot}4 \times 10^{-4}$ mol/(m^2s) at 1000 K using a $TiCl_4$ input concentration of 0·268 mol/m^3. A relatively high surface growth rate constant or a relatively high reactant is beneficial for the amount of deposited mass within the pore network as can be illustrated by the model

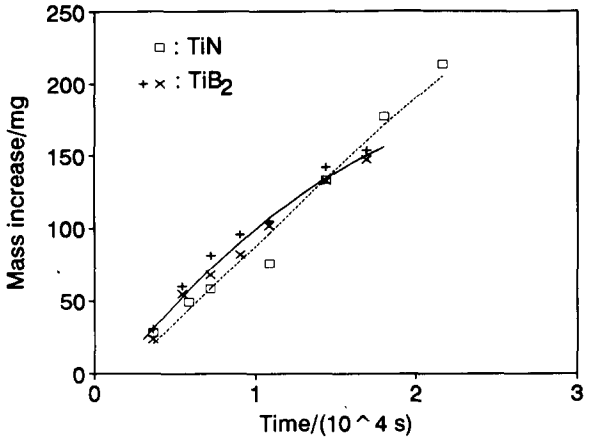

Fig. 5. Measured mass increase of TiB_2 and TiN modified substrates as a function of process time.

calculations for the deposition of TiB_2 in a cylinder presented in Figs 6 and 7. Apparently, the combination of these experimental parameters will lead to similar densifications. The observed decrease in the slope of the mass increase for the TiB_2 experiments is a consequence of the high growth rate which will reduce the initial pore size and increase the mass flux resistance of the pore network. It is expected that the TiB_2 deposit is concentrated near the pore entrance, whereas a more uniform deposition in the pore network is expected for the TiN experiments. Thus, at long process times the final densification of TiN will be higher than the final densification of TiB_2 given these process conditions.

The expected strong decrease in the amount of deposited TiB_2 inwards the substrate for different process times is confirmed by the EDX analysis as can be seen in Fig. 8. Similar deposition profiles as a function of time are found for the TiB_2 model calculations as can be seen in Fig. 9. The infiltration depth defined as the position where the deposit thickness is half of the deposit thickness at the outside remains unchanged as a function of

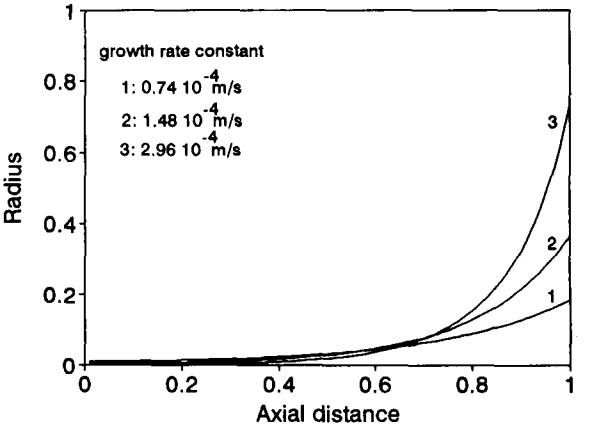

Fig. 6. Predicted deposition profiles of TiB_2 in a small cylinder for different growth rate constants. The axial distance ranges from the middle of the cylinder (0) to the outside of the cylinder (1).

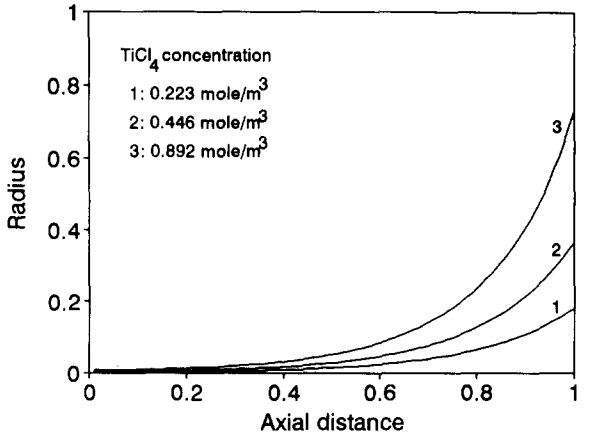

Fig. 7. Predicted deposition profiles of TiB_2 in a small cylinder for different $TiCl_4$ concentrations. The axial distance ranges from the middle of the cylinder (0) to the outside of the cylinder (1).

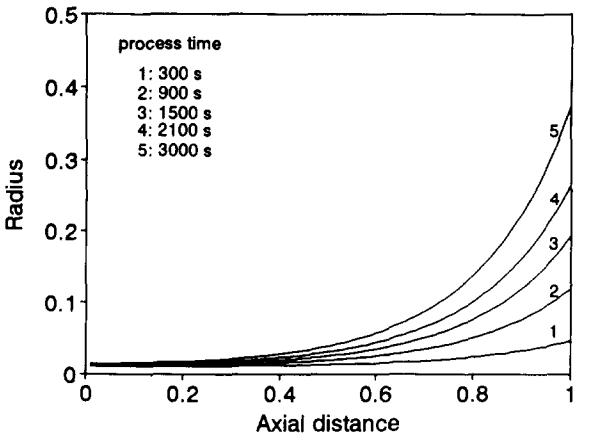

Fig. 9. Predicted deposition profiles of TiB_2 in a small cylinder for different process times. The axial distance ranges from the middle of the cylinder (0) to the outside of the cylinder (1).

process time and reactant concentration as can be seen in Figs 7 and 9. This phenomenon is typical for a growth rate which has a first order dependence in the reactant concentration[15,16] Thus, given the EDX analysis results as presented in Fig. 8 the assumption is justified that the growth rate for TiB_2 is first order with respect to the reactant concentration.

The TiN deposition profiles at different $TiCl_4$ concentrations in porous Al_2O_3 obtained from the EDX analysis presented in Fig. 10 differ from the predicted deposition profiles for first order reaction kinetics presented in Fig. 9. The TiN growth rate expression has a complex dependence on the reactant concentration: it can be described by an adsorption–reaction mechanism based on an isothermal Langmuir adsorption behaviour.[17,23,24] At high $TiCl_4$ concentration such an adsorption–reaction mechanism predicts for the growth rate a negative order dependence in the $TiCl_4$ concentration.[17,23,24] As a consequence, the infiltration depth increases with increasing $TiCl_4$ concentration. A more detailed discussion of the influence of such a growth rate mechanism on the densification is given elsewhere.[15,16]

Permeability

The proposed dependence for the permeability on the pressure has been validated by measuring the flow rate through the substrate as a function of pressure for argon and helium. In all cases, the data could be fitted according to eqn (3). The relative argon permeability of the TiB_2 modified substrates as a function of the densification (X) is presented in Fig. 11. The permeability of the substrates synthesized at a reactor pressure of 10^5 Pa shows a stronger dependence on X than the permeability of the substrates synthesized at a reactor pressure of 5×10^4 Pa. The deposit is more uniformly distributed in the pore network at a reactor pressure of 5×10^4 Pa than at a reactor pressure of 10^5 Pa, because, at low reactor pressures the growth rate constant is smaller than at higher reactor pressures which favours the infiltration as

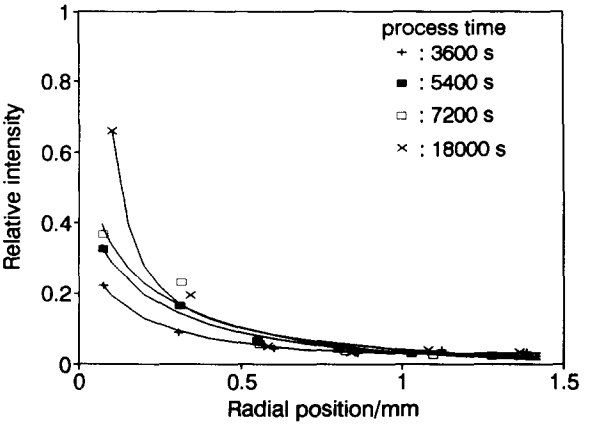

Fig. 8. Deposition profiles of TiB_2 as derived from the EDX analysis for different process times. The radial position is relative to the outside of the substrate. The substrates are synthesized at a reaction temperature of 1000 K, and a reactor pressure of 5×10^4 Pa.

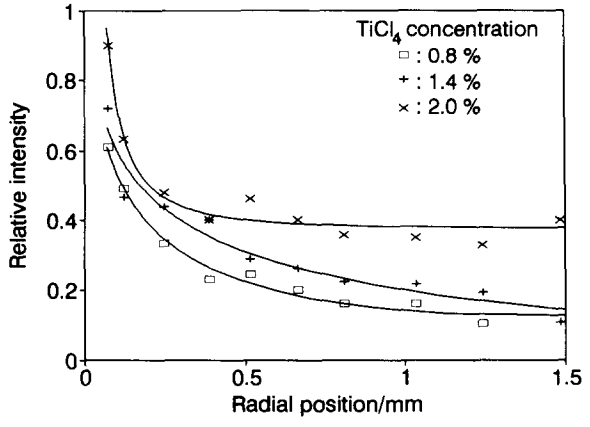

Fig. 10. Deposition profiles of TiN as derived from the EDX analysis at different $TiCl_4$ concentrations. The radial position is relative to the outside of the substrate. The substrates are synthesized at a reaction temperature of 1123 K and a process time of 3600 s.

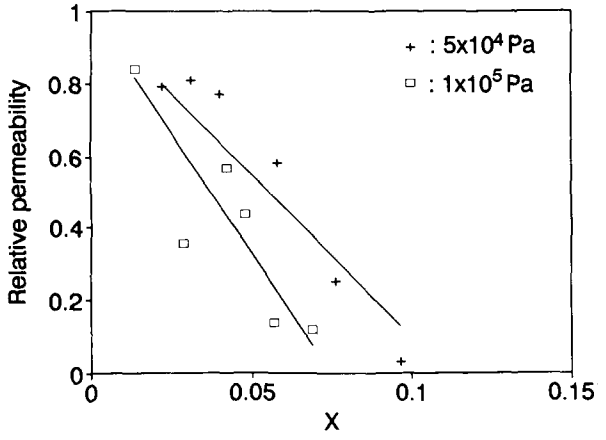

Fig. 11. Relative argon permeability for TiB_2 modified substrates as a function of the densification (X). The substrates are synthesized at a reaction temperature of 1000 K, a process time of 3600 s, and a reactor pressure of 5×10^4 or 10^5 Pa.

can be seen for the model predictions presented in Fig, 6. Moreover, the diffusion of the reactants in the gas phase increases with decreasing reactor pressure. From these considerations it can be concluded that the permeability decreases less with increasing densification if the deposited mass is more uniformly distributed within substrate. A similar argument can be given for the permeability of the TiN modified substrates synthesized at different reaction temperatures. At a high reaction temperature the deposited mass in the substrate is located near the entrance of the pore network, whereas at low reaction temperatures the mass is more uniformly distributed. Thus, the decrease in permeability as a function of X is stronger for the substrates synthesized at 1123 K than at 1073 K as can be seen in Fig. 12.

Mechanical testing

The diametral C-ring compression testing results indicate that there is a considerable increase in the relative strength with increasing densification for

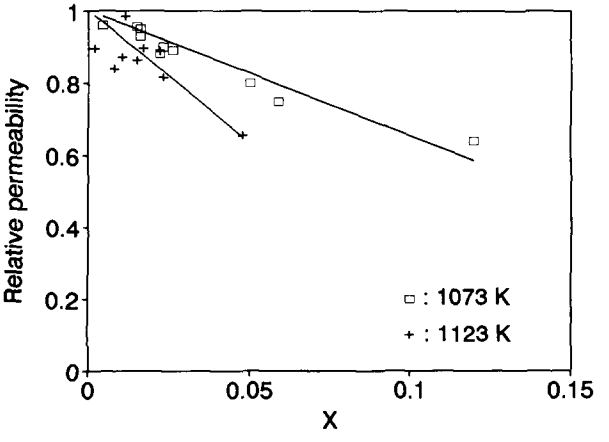

Fig 12. Relative argon permeability for TiN modified substrates as a function of the densification (X). The substrates are synthesized at a $TiCl_4$ input concentration of 0·446 mol/m^3, a process time of 3600 s, and a reaction temperature of 1073 or 1123 K.

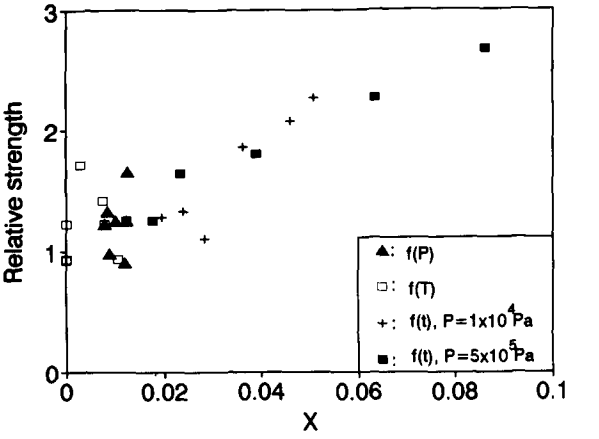

Fig 13. Relative strength of TiB_2 modified substrates as derived from the C-ring compression tests.

the TiB_2 and TiN modified substrates as can be seen in Figs 13 and 14, respectively. The scattering in the results of the C-ring tests has to be attributed to the failure probability of the original substrate and to an unknown influence of the modification on the failure probability. The average maximum stress at failure is 7·35 ± 0·98 MPa for the untreated substrates. The failure probability for the C-ring compression test can be evaluated by Weibull statistics. The tangential stresses in a compressed C-ring for an isotropic material are significantly larger than either the radial or the shear stresses at the outside of the specimen.[20] Thus, the two parameter Weibull equation for the failure probability can be used considering only the tangential stresses[20]

$$-\ln(1-P) = \left(\frac{\sigma_\theta^{\max}}{\sigma_0}\right)^m \int_{V/2} \left(\frac{\sigma_\theta}{\sigma_\theta^{\max}}\right)^m \times r\, \mathrm{d}(r)\, \mathrm{d}(\theta)\, \mathrm{d}(l) \qquad (8)$$

where P is the probability of failure, $\sigma_\theta^{\max}$ is the maximum tensile stress, σ_0 is a scaling parameter, and m is the Weibull modulus. The integral is evaluated over the volume of the substrate, because it is assumed that the strength of this type

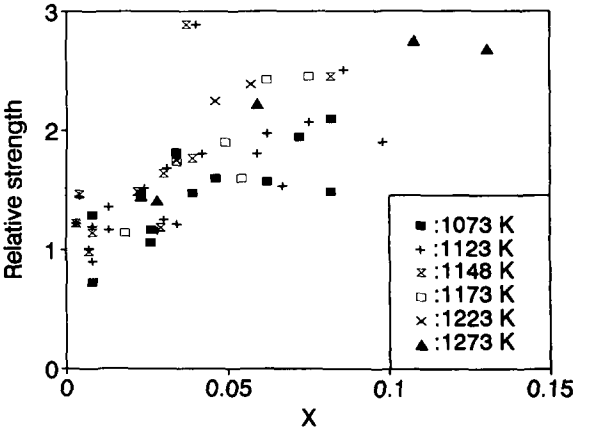

Fig 14. Relative strength of TiN modified substrates as derived from the C-ring compression tests.

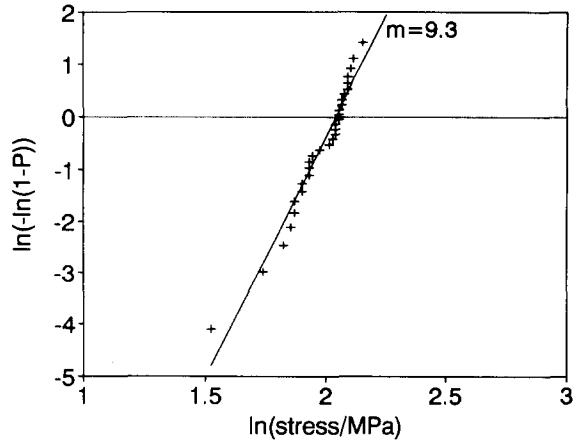

Fig. 15. Weibull plot for the results of the C-ring compression test of the untreated substrates.

of porous structure is determined by a volume controlled failure.[11,22] The volume integral, i.e. a measure for the effective volume can be defined[20]

$$\int_{V/2} \left(\frac{\sigma_\theta}{\sigma_\theta^{\max}}\right)^m r\, \mathrm{d}(r)\, \mathrm{d}(\theta)\, \mathrm{d}(l)$$

$$= Lr_a^2 \left[2 \int_0^{\pi/2} \cos^m(\theta)\, \mathrm{d}(\theta)\right]$$

$$\times \left[\int_1^{r_o/r_a} \left(\frac{1 - 1/x}{1 - r_a/r_o}\right)^m x\, \mathrm{d}(x)\right] \qquad (9)$$

where x is a dummy for integration. The C-ring compression results for 30 untreated specimens are fitted to the two parameter Weibull eqn (8) using for the failure probability the expression

$$P = \frac{n - 0{\cdot}5}{N} \qquad (10)$$

where n is the rank of a particular specimen and N is the total number of substrates tested. The Weibull plot for the untreated substrates is presented in Fig. 15. The Weibull modulus of the least squares fit is 9·3 and the scaling parameter is 1·33 MPa (times unit volume). A similar quantitative weakest link analysis for the modified substrates is not possible, because of the unknown stress distribution. In addition, the densities of the substrates are different, because each substrate is modified at different process conditions. However, a more qualitative analysis can be applied by defining a normalized strength. This normalized strength corrects for the densification. After this normalization all modified substrates, i.e. 28 specimens for TiB_2 and 76 specimens for TiN can be used for the weakest link analysis.

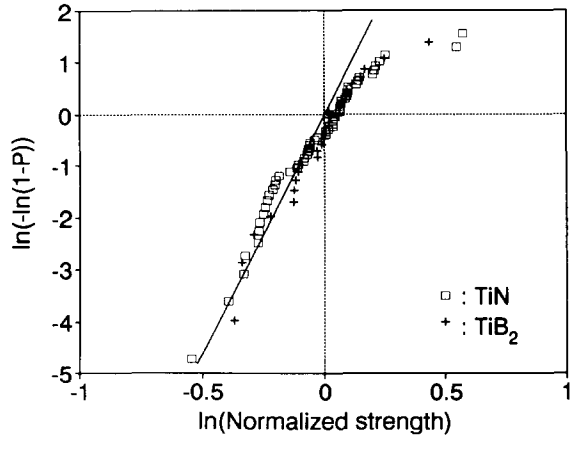

Fig. 16. Weibull plot for the failure distribution of the modified substrates. The solid line represents the failure distribution of the untreated substrates.

It is assumed that the strengthening of the material is proportional to the densification (X)

$$\sigma_X = C_3 + C_4 X \qquad (11)$$

where C_3 and C_4 are fit constants and σ_X is the calculated strength at a densification (X) using eqns (4)–(7). Equation (11) satisfies the boundary condition at $X = 0$ if constant C_3 is equal to the average strength of the untreated substrates. To our knowledge there are no reports on satisfactory relationships between the strength and porosity for anisotropic composite materials. However, for ceramic materials with small pore fractions a linear equation has been attempted earlier to describe the mechanical properties as a function of the porosity.[2,25,26] The normalized strength for TiN and TiB_2 can be defined as the ratio of the calculated $\sigma_\theta^{\max}$ over the right-hand side of eqn (11). The constants C_3 and C_4 for TiB_2 and TiN are obtained by a linear regression fit of the data presented in the Figs 13 and 14, respectively. The denominator of the normalized strength acts as the scaling parameter of the Weibull statistics if this normalized strength is used for the failure probability analysis. The Weibull plot for the failure distribution of the normalized strength is given in Fig. 16. The solid line represents the predicted failure distribution for the untreated substrates. The failure distribution of the modified substrates is comparable to the untreated substrates. This suggests that the modification has not a negative influence on the failure probability.

Hitherto, the densification (X) is considered as the only contribution to the improvement in strength. However, not only the densification but also the distribution of the deposit in the pore net-

Table 4. Fit constants of the strengthening eqn (11) for Al_2O_3 substrates modified with TiB_2 as a function of process time at two reactor pressures

Fit constants	*Reactor pressure (10^4 Pa)*		
	5	10	
C_3	7·64 ± 0·56	5·60 ± 1·60	MPa
C_4	142 ± 12	201 ± 48	MPa

Table 5. Fit constants of the strengthening eqn (11) for Al_2O_3 substrates modified with TiN as a function of process time at different temperatures

Fit constants	*Reaction temperature (K)*						
	1073	*1123*	*1148*	*1173*	*1223*	*1273*	
C3	7·53 ± 1·98	8·43 ± 2·82	8·42 ± 3·82	5·90 ± 1·85	6·43 ± 0·97	8·93 ± 1·67	MPa
C4	79 ± 22	87 ± 22	135 ± 46	162 ± 41	202 ± 61	94 ± 17	MPa

work is of importance. This can be illustrated by the fit results of eqn (11) for the substrates synthesized as a function of time, because the shape of the deposition profile remains unchanged as a function of process time if the reaction is determined by first order kinetics. The fit results for eqn (11) for the TiB_2 and TiN modified substrates are presented in Tables 4 and 5, respectively.

The boundary condition for eqn (11) at $X = 0$ is fulfilled for all experiments. Constant C_4 is a measure for the increase in strength with increasing densification. There tends to be an increase in C_4 with increasing reaction temperature or reactor pressure. This originates from the fact that at high reaction temperatures or reactor pressures most of the material is deposited in the pore network near the outside of the substrate, and in the mechanical C-ring compression tests the resulting stresses are the highest at the outside of the material. Thus, the material deposited near the outside is more effective for strengthening of the substrate than the material deposited in the central part of the substrate. As mentioned above it is assumed that the failure is volume controlled. However, the presented results can not exclude the presence of surface controlled failure. Other mechanical testing configurations should be applied in order to be more conclusive on the precise nature of the improvement in strength after modification.

Conclusions

Porous alumina substrates can effectively be modified with TiN or TiB_2. The amount of deposited material in the substrate is determined by a combination of growth rate constant, reactant concentration, diffusion, and process time. The model predictions indicate that a low growth rate constant and a high diffusion are beneficial for the infiltration of the deposit into the substrate. For first-order reaction kinetics the dependence of the infiltration characteristics on process time and reactant concentration are similar. A high process time or reactant concentration enhances the densification. However, the infiltration depth remains unchanged. This predicted behaviour is confirmed by the EDX analysis for the deposition of TiB_2. In contrast, the infiltration depth increases with increasing reactant concentration for the deposition of TiN. This has to be ascribed to a complex growth rate dependence on the reactant concentration which is not first order for the deposition of TiN.

The permeability of the modified substrates decreases with increasing densification. The decrease in the permeability is not only a function of the total amount of deposited material within the substrate but also of the distribution of the deposited material in the substrate. If the deposit is uniformly distributed within the pore network, i.e. at low reaction temperature and reactor pressure, then the densification has a small influence on the permeability. The decrease in permeability is far more affected by the pore narrowing at the outside of the substrate.

The strength of the substrate can be enhanced considerably with the CVI process. Approximately, a densification of 5% relative to the original porosity can double the strength of the substrate. A qualitative weakest link analysis indicates that the modification has not a negative influence on the failure distribution of the C-ring compression test results. The results from the C-ring compression tests indicate that the increase in strength with increasing densification is less pronounced for the experiments where the deposit is uniformly distributed within the substrate.

Thus, a uniform distribution is favourable for a good permeability whereas a deposit in the pore network which is concentrated near the outside of the substrate gives a better improvement in the strength for a compressed C-ring.

References

1. Hsieh, H. P., Inorganic membrane reactors, a review. *AlChE*, **268** (1989) 53–67.
2. Hsieh, H. P., Inorganic membrane reactors. *Catal. Rev.-Sci Engng.*, **33** (1991) 1–70.
3. Coble, R. L & Kingery, D., Effect of porosity on physical properties of sintered alumina. *J. Am. Ceram. Soc.*, **39** (1956) 377–85.
4. Nielsen, L. F., Strength and stiffness of porous materials. *J. Am. Ceram. Soc.*, **73** (1990) 2684–9.
5. Phani, K. K., Niyogi, S. K. & De, A. K., Porosity dependence of fracture mechanical properties of reaction sintered Si_3N_4. *J. Mater. Sci. Lett.*, **7** (1988) 1253–6.

6. Krstic, V. D., Porosity dependence of strength in materials. In *Proc. Int. Symp. on Advanced Structural Materials*, ed. D. S. Wilkinson. Pergamon Press, Oxford, UK, 1988, pp. 115–21.
7. Pierson, H. O., *Handbook of Chemical Vapour Deposition (CVD)*, Noyes Publications, Park Ridge, 1992.
8. Spear, K. E. & Dirkx, R. R., Role of high temperature chemistry in CVD processing. *Pure Appl. Chem.*, **62** (1990) 89–101.
9. Besmann, T. M., Lowden, R. A., Sheldon, B. W. & Stinton, D. P., Chemical vapor infiltration. In *Proc. 11th Int. Conf. on Chemical Vapor Deposition* (Vol. 90–12), eds K. E. Spear & G. W. Cullen. The Electrochemical Society, Pennington, 1990, pp. 482–91.
10. Terpstra, R. A., Bonekamp, B. C. & Veringa, H. J., Preparation, characterization and some properties of tubular alpha alumina ceramic membranes for microfiltration and as a support for ultrafiltration and gas separation membranes. *Desalination*, **70** (1988) 395–404.
11. Terpstra, R. A., Visser, H. H., Engel, A. J. G. & Veringa, H. J., Structural properties of ceramic alumina microfiltration membranes as a function of sintering time and temperature. In *Proc. First European Ceramic Society Conf., Euro Ceramics* (Vol. 3), eds G. de With, R. A. Terpstra & R. Metselaar. North Holland, The Netherlands, 1989, pp. 615–19.
12. Radovich, J. M., Behnam, B. & Mullon, C., Steady-state modelling of electro-ultrafiltration at constant concentration. *Separation Sci. Technol.*, **20** (1985) 315–29.
13. Radovich, J. M. & Chao, I. M., Electro-ultrafiltration of a cationic electrodeposition paint. *J. Coatings Technol.*, **54** (1982) 33–40.
14. Lin, Y. S., Analysis of CVI process of porous material densification using a continuous model. In *Proc. 11th Int. Conf. on Chemical Vapor Deposition*, Vol 90–12, eds. K. E. Spear & G. W. Cullen. The Electrochemical Society, Pennington, 1990, pp. 532–8.
15. Moene, R., Dekker, J. P., Makkee, M., Schoonman, J. & Moulijn, J. A., Evaluation of isothermal chemical vapor infiltration with Langmuir–Hinshelwood type kinetics. *J. Electrochem. Soc.*, **141** (1993) 282–90.
16. Dekker, J. P., Moene, R., Veringa, H. J. & Schoonman, J., The importance of surface kinetics in modelling chemical vapour deposition processes in porous preforms. *J. Mat. Sci.*, submitted, (1994).
17. Dekker, J. P., van der Put, P. J., Veringa, H. J. & Schoonman, J., A kinetic study of titanium nitride chemical vapour deposition using nitrogen, hydrogen, and titanium tetrachloride. *J. Electrochem. Soc.*, **141** (1993) 787–95.
18. Dekker, J. P., van der Put, P. J., Veringa, H. J. & Schoonman, J., Chemical vapour deposition of titanium diboride using boron tribromide, titanium tetrachloride, and hydrogen. *J. CVD*, **1** (1993) 317–32.
19. Methods of Test for Ceramic Coatings, CEN/TC 184 N78, 1992.
20. Ferber, M. K., Tennery, V. J., Waters, S. B. & Ogle, J., Fracture strength characterization of tubular materials using a simple C-ring geometry. *J. Mater. Sci.*, **21** (1986) 2628–32.
21. Cernica, J. N., *Strength of Materials*. Holt, Reinhart and Winston, New York, 1966 p. 201.
22. Bach, P. W., van der Burg, N. P. G. & Terpstra, R. A., Mechanical characterization of macroporous support tubes for micro/ultrafiltration. In *Proc. First European Ceramic Society Conf., Euro Ceramics* (Vol. 3), eds. G. de With, R. A. Terpstra & R. Metselaar. North Holland, The Netherlands, 1989, pp. 575–82.
23. Rong, C. Z., Sheng, D. Y. & Fang, M. H., Kinetics and mechanisms of TiN chemical vapour deposition in Ti–Cl–H–N system. *Surf. Engng.*, **5** (1989) 315–22.
24. Nakanishi, N., Mori, S. & Kato, E., Kinetics of chemical vapor deposition of titanium nitride. *J. Electrochem. Soc.*, **137** (1990) 322–8.
25. Dean, E. A. & Lopez, J. A., Empirical dependence of elastic moduli on porosity for ceramic materials. *J. Am. Ceram. Soc.*, **66** (1983) 366–70.
26. Nielsen, L. F., Elasticity and damping of porous materials and impregnated materials. *J. Am. Ceram. Soc.*, **67** (1984) 93–8.